Dear Daniel Fisher,

Thank you very much for your valuable comments. We have followed your suggestions and we find that our paper is now improved in general and more thoroughly compared with the most recent literature on the subject.

In this document, your original comments are framed by a box and our answer follows.

In this paper the thermal anomaly detection and characterisation algorithm developed in Casiero et al. (2018), based on NightFire, is applied to Sentinel-3 SLSTR data with the objective of evaluating global gas flaring radiant heat output and the associated estimates of black carbon emissions. The resulting thermal anomaly outputs, generated for 2017, are subjected to various filters to partition flaring and non-flaring anomalies, with the most crucial step being the application of a persistency test of more than five observations in the 12 month evaluation period in addition to a minimum temperature limit of 1500 K, which must be exceeded. A normalisation process is then applied to the detected gas flaring sites to account for differences in sampling opportunities to generate an adjusted measure of radiant heat output for each flaring site. Black carbon emissions estimates are then generated from the adjusted radiant heat estimates using appropriate emission factors. Finally comparison against various other datasets are made to assess the validity of the SLSTR generated datasets.

Whilst in general the paper is reasonably well written, there is a potentially significant flaw in the gas flare characterisation approach which must be investigated and addressed before publication can be recommended. In Elvidge et al. (2016) and Fisher et al. (2019) it is demonstrated that a substantial proportion of global gas flaring radiant heat output arises from a small subset of flaring sites global (50% of output comes from 5-10% of all flares). Some of these flares are extremely radiant such as the Punta de Mata site in Venezuela identified by the authors (and elsewhere), and they attribute 0.623 BCM of flared gas to this site in 2017. In comparison, Elvidge et al (2016) identified that 1.13 BCM of gas was flared at this site in 2012. The discrepancy between these two values is concerning, particularly as Venezuela has been shown to have had a very large increase in gas flare radiant heat output since 2012 (Fisher et al., 2019), and given the characteristics of gas flaring (e.g. most radiant heat being produced by a small subset of sites) one would expect that the most active flaring site in Venezuela to have show at least some increase, and not the reported decrease.

I think that this result may be arising from a potential issue with the channels used by the algorithm. In Elvidge et al. (2019) the issue of saturation in the (M11) 2.2 m and (M12) 3.7 m VIIRS channels is identified and I would expect that a similar issue is occurring with SLSTR, particularly given the enhancement in pixel resolution from 750 m2 to 500 m2. The channels employed in the Casiero et al. (2018) for the estimation of gas flare radiant heat output are S5 (1.6 µm), S6 (2.2 µm) and S7/F1 (3.7 µm). Given its specifications, the S7 channel likely saturates on a regular basis over gas flares, and this is identified, as is the potential for using the F1 channel when this occurs. However, no assessment of the saturation characteristics of the SWIR channels is made, and whilst the S5 channel likely does not saturate, the same cannot be said for the S6 channel. Furthermore, being a relatively new instrument the performance of the F1 channel has not been evaluated, and it needs to be demonstrated that it reaches the specified dynamic range performance levels (the same can be said for the SWIR channels). If any of the channels are saturating then the effects on the retrieved radiant heat can be significant as shown in Elvidge et al. (2019), and in the current configuration of the algorithm used in this paper these saturation events may well be being missed. I expect, given that a significant proportion of radiant heat output arises from a subset of highly radiant flaring sites, the impact of saturation on the reported global total of radiant heat output and in turn BCM could well be significant and must be explored.

To do so I would recommend:

(1) evaluating the Planck curves of the most radiant flare sites identified globally and check the deviations of the various spectral observations from the curves that might indicate saturation of specific channels, giving at least an indication of saturation effects on SLSTR.

We already address the reviewer's concern of S7 and S9 saturation by using F1 and F2 when necessary (see also Caseiro et al. 2018). Saturation of the SWIR channels do not lead to a good fit and do not converge. Please find all the Planck curve fits within the most active flaring location at the end of this document.

(2) I would recommend applying the single channel radiant heat estimation approach of Fisher and Wooster (2018) developed in part for application to the S5 channel of the SLSTR sensor and see if any significant differences are observed, this would be a very straightforward comparison.

We added a new subsection where we apply the single SWIR method (Fisher and Wooster 2018 and 2019) to our detections and compare the results in terms of radiative power (RP), see figure below. We also compare our results with the results from Fisher and Wooster 2019. This shows that our method is biased high compared to the SWIR method and also gives larger maximum FRP values. Therefore, the FRP calculation should not lead to a low bias for the largest gas flares as suspected by the reviewer.

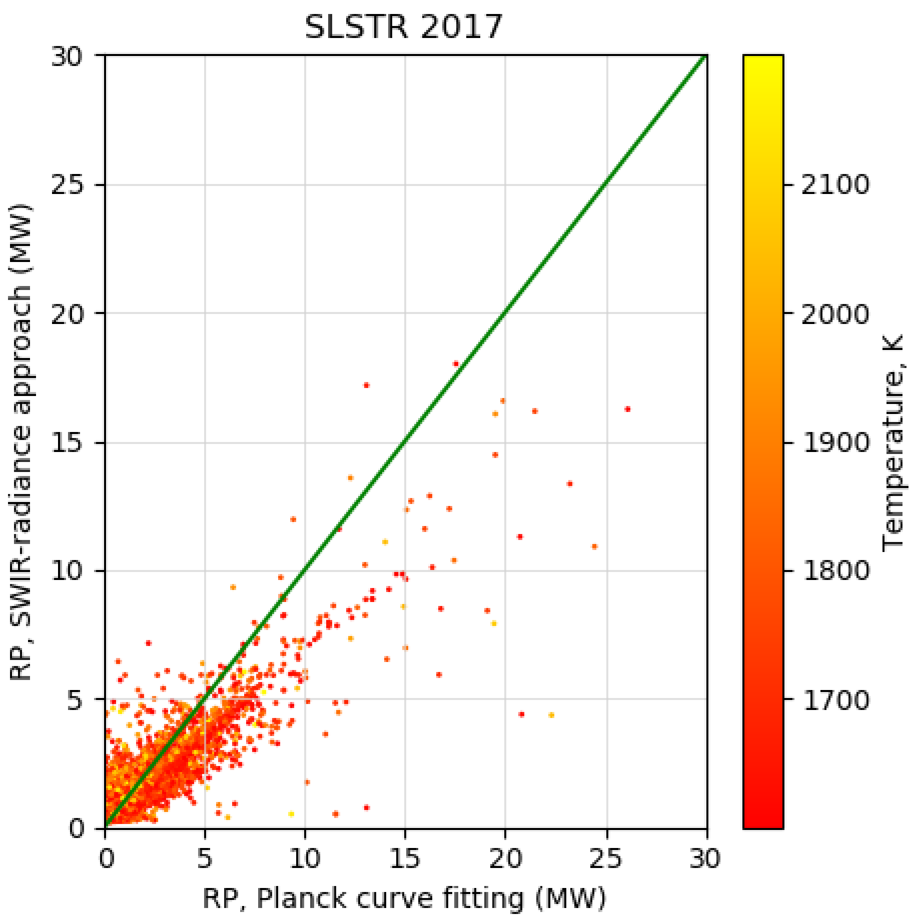

(3) I would then suggest that if a discrepancy for these larger flaring sites is found that the S3 channel is included as an additional constraint for these very large flares to try and improve the radiant heat estimates.

The NIR channels S3 (0.865 µm) and/or S4 (1.375 µm) are strong candidates to constrain more precisely the dual Planck curve fit. Both these channels are turned off at night, but during the commissioning phase of the satellite, which corresponded to the development phase of our methodology, they were switched on at night by ESA for a limited time period. Our conclusions were that the signal-to-noise ratio was too low for extracting additional information.

(4) It would be likely be useful to compare also against flare counts from Fig. 7 in Fisher and Wooster (2019) in addition to the NightFire comparison.

This has been added to the manuscript, see answer to recommendation #2.

Lastly, some key references are missing from the paper and should be included:

Anejionu, O.C., 2019. Rationale, historical developments and advances in remote sensing of gas flares. International Journal of Remote Sensing, 40(17), pp.6700-6719.

Elvidge, C.D., Zhizhin, M., Baugh, K., Hsu, F.C. and Ghosh, T., 2019. Extending nighttime combustion source detection limits with short wavelength VIIRS data. Remote Sensing, 11(4), p.395.

Fisher, D. and Wooster, M., 2018. Shortwave IR Adaption of the Mid-Infrared Radiance Method of Fire Radiative Power (FRP) Retrieval for Assessing Industrial Gas Flaring Output. Remote Sensing, 10(2), p.305.

Fisher, D. and Wooster, M.J., 2019. Multi-decade global gas flaring change inventoried using the ATSR-1, ATSR-2, AATSR and SLSTR data records. Remote Sensing of Environment, 232, p.111298.

1 + 2 + 4 were not originally included because they came out after or towards the end of the time of writing. All four are now cited in the paper.

Other references referred to here:

Caseiro, A., Rücker, G., Tiemann, J., Leimbach, D., Lorenz, E., Frauenberger, O. and Kaiser, J., 2018. Persistent Hot Spot Detection and Characterisation Using SLSTR. Remote Sensing, 10(7), p.1118.

Elvidge, C. D., Zhizhin, M., Baugh, K., Hsu, F.-C., and Ghosh, T.: Methods for Global Survey of Natural Gas Flaring from Visible Infrared Imaging Radiometer Suite Data, Energies, 9, 14,

Planck curve fits at the most active flaring location:

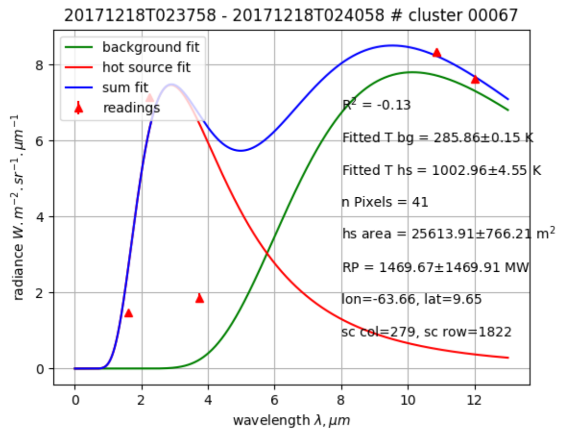

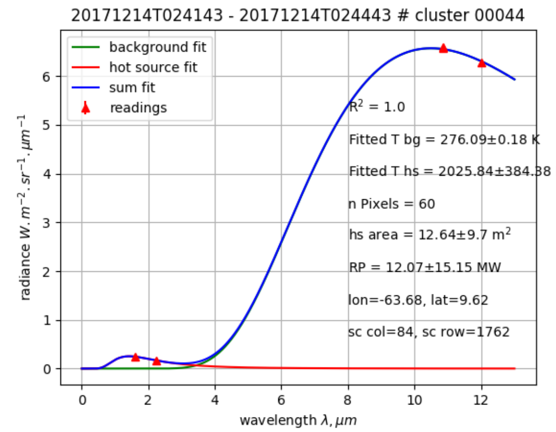

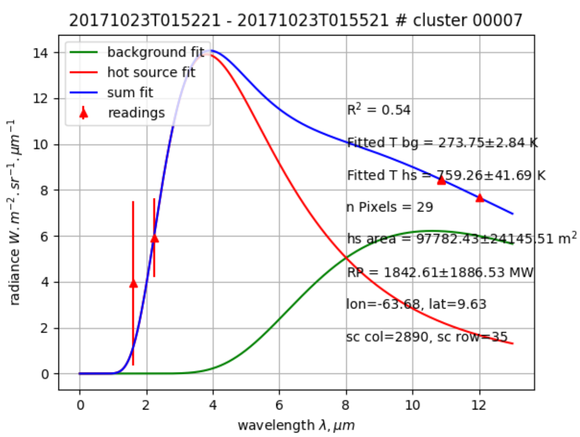

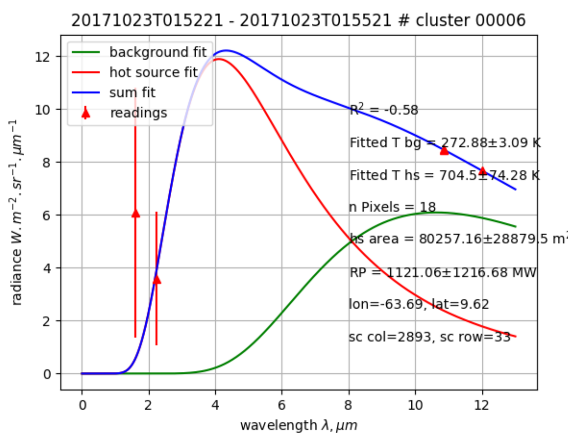

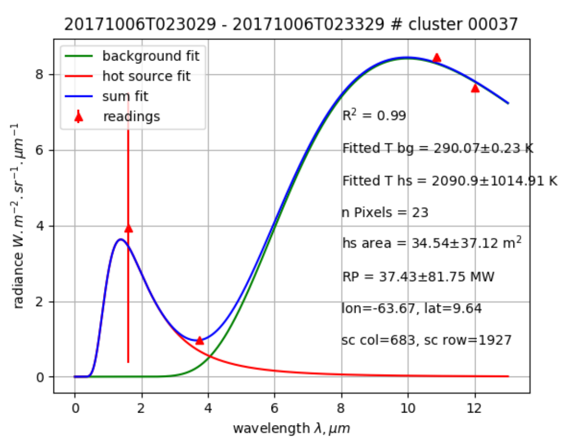

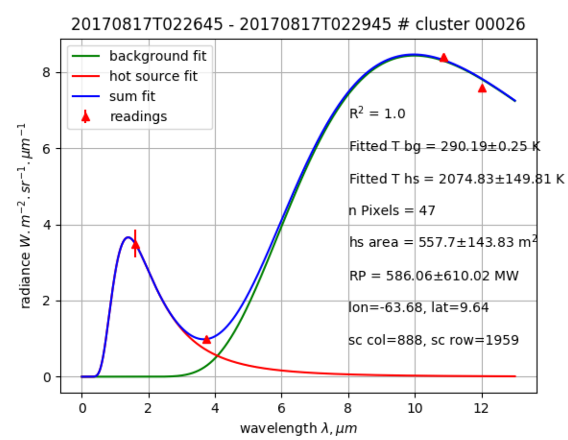

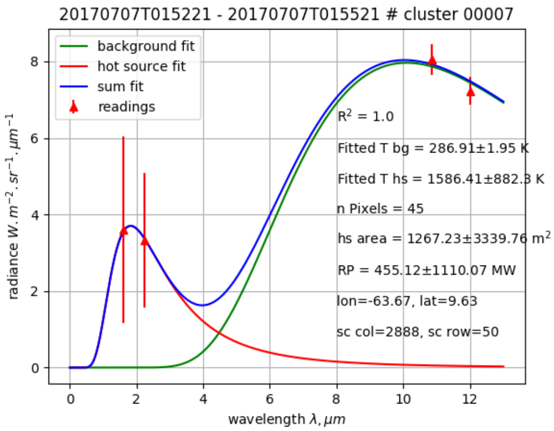

20170707T015221 - 20170707T015521 # cluster 00007
background fit
hot source fit
sum fit
readings
R^2 = 1.0
Fitted T bg = 286.91±1.95 K
Fitted T hs = 1586.41±882.3 K
n Pixels = 45
hs area = 1267.23±3339.76 m^2
RP = 455.12±1110.07 MW
lon=-63.67, lat=9.63
sc col=2888, sc row=50
radiance $W.m^{-2}.sr^{-1}.\mu m^{-1}$
wavelength $\lambda, \mu m$

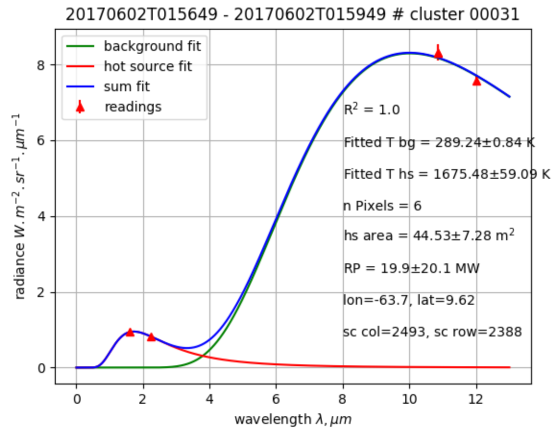

20170602T015649 - 20170602T015949 # cluster 00031
background fit
hot source fit
sum fit
readings
R^2 = 1.0
Fitted T bg = 289.24±0.84 K
Fitted T hs = 1675.48±59.09 K
n Pixels = 6
hs area = 44.53±7.28 m^2
RP = 19.9±20.1 MW
lon=-63.7, lat=9.62
sc col=2493, sc row=2388
radiance $W.m^{-2}.sr^{-1}.\mu m^{-1}$
wavelength $\lambda, \mu m$

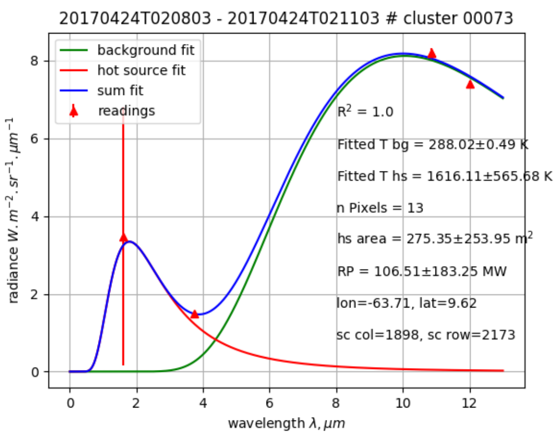

20170424T020803 - 20170424T021103 # cluster 00073
background fit
hot source fit
sum fit
readings
R^2 = 1.0
Fitted T bg = 288.02±0.49 K
Fitted T hs = 1616.11±565.68 K
n Pixels = 13
hs area = 275.35±253.95 m^2
RP = 106.51±183.25 MW
lon=-63.71, lat=9.62
sc col=1898, sc row=2173
radiance $W.m^{-2}.sr^{-1}.\mu m^{-1}$
wavelength $\lambda, \mu m$

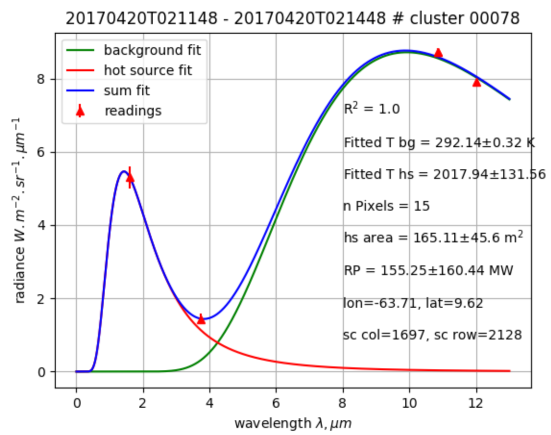

20170420T021148 - 20170420T021448 # cluster 00078
background fit
hot source fit
sum fit
readings
R^2 = 1.0
Fitted T bg = 292.14±0.32 K
Fitted T hs = 2017.94±131.56 K
n Pixels = 15
hs area = 165.11±45.6 m^2
RP = 155.25±160.44 MW
lon=-63.71, lat=9.62
sc col=1697, sc row=2128
radiance $W.m^{-2}.sr^{-1}.\mu m^{-1}$
wavelength $\lambda, \mu m$

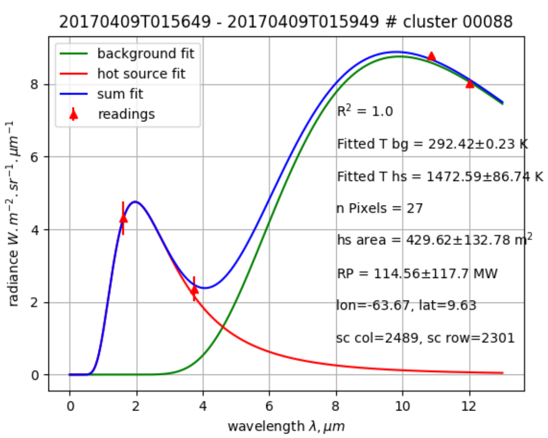

20170409T015649 - 20170409T015949 # cluster 00088
background fit
hot source fit
sum fit
readings
R^2 = 1.0
Fitted T bg = 292.42±0.23 K
Fitted T hs = 1472.59±86.74 K
n Pixels = 27
hs area = 429.62±132.78 m^2
RP = 114.56±117.7 MW
lon=-63.67, lat=9.63
sc col=2489, sc row=2301
radiance $W.m^{-2}.sr^{-1}.\mu m^{-1}$
wavelength $\lambda, \mu m$

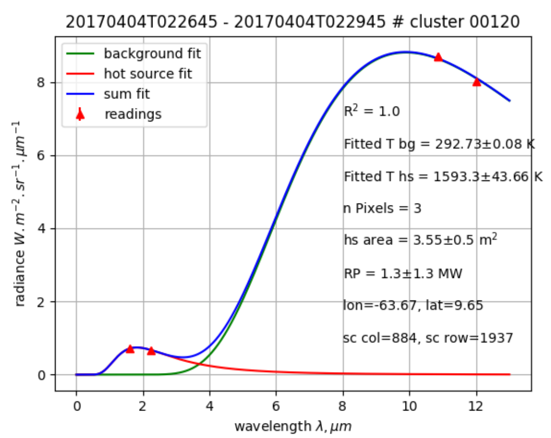

20170404T022645 - 20170404T022945 # cluster 00120
background fit
hot source fit
sum fit
readings
R^2 = 1.0
Fitted T bg = 292.73±0.08 K
Fitted T hs = 1593.3±43.66 K
n Pixels = 3
hs area = 3.55±0.5 m^2
RP = 1.3±1.3 MW
lon=-63.67, lat=9.65
sc col=884, sc row=1937
radiance $W.m^{-2}.sr^{-1}.\mu m^{-1}$
wavelength $\lambda, \mu m$

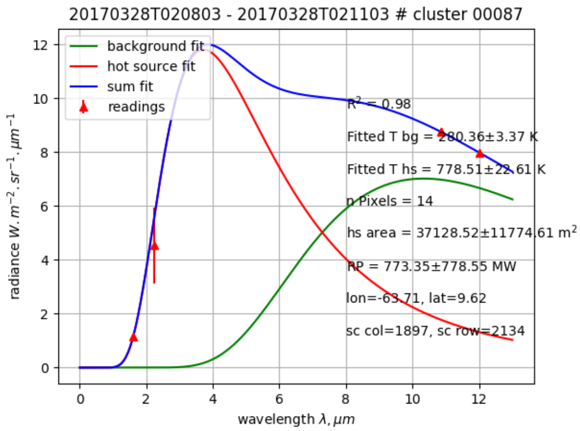
20170328T020803 - 20170328T021103 # cluster 00087
background fit
hot source fit
sum fit
readings
R^2 = 0.98
Fitted T bg = 280.36±3.37 K
Fitted T hs = 778.51±22.61 K
n Pixels = 14
hs area = 37128.52±11774.61 m^2
RP = 773.35±778.55 MW
lon=-63.71, lat=9.62
sc col=1897, sc row=2134
radiance $W.m^{-2}.sr^{-1}.\mu m^{-1}$
wavelength $\lambda, \mu m$

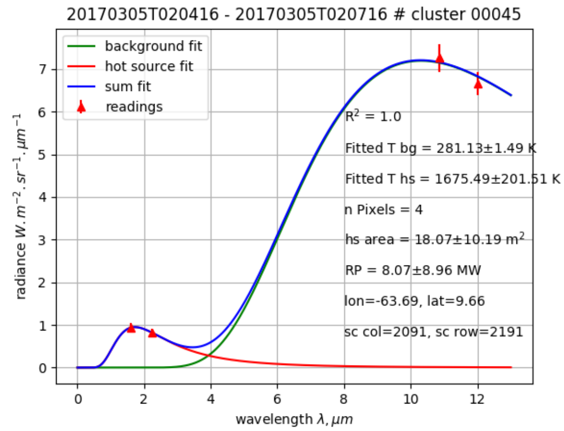
20170305T020416 - 20170305T020716 # cluster 00045
background fit
hot source fit
sum fit
readings
R^2 = 1.0
Fitted T bg = 281.13±1.49 K
Fitted T hs = 1675.49±201.51 K
n Pixels = 4
hs area = 18.07±10.19 m^2
RP = 8.07±8.96 MW
lon=-63.69, lat=9.66
sc col=2091, sc row=2191
radiance $W.m^{-2}.sr^{-1}.\mu m^{-1}$
wavelength $\lambda, \mu m$

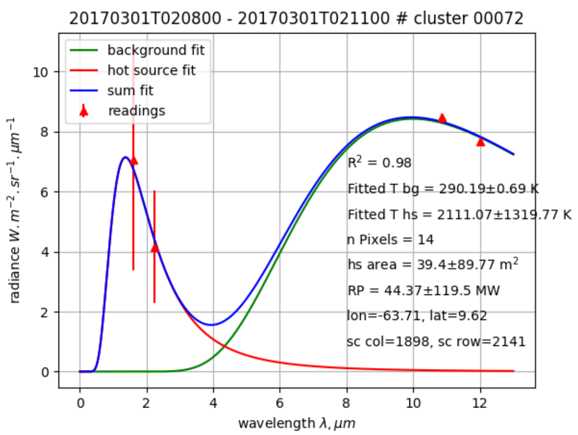
20170301T020800 - 20170301T021100 # cluster 00072
background fit
hot source fit
sum fit
readings
R^2 = 0.98
Fitted T bg = 290.19±0.69 K
Fitted T hs = 2111.07±1319.77 K
n Pixels = 14
hs area = 39.4±89.77 m^2
RP = 44.37±119.5 MW
lon=-63.71, lat=9.62
sc col=1898, sc row=2141
radiance $W.m^{-2}.sr^{-1}.\mu m^{-1}$
wavelength $\lambda, \mu m$

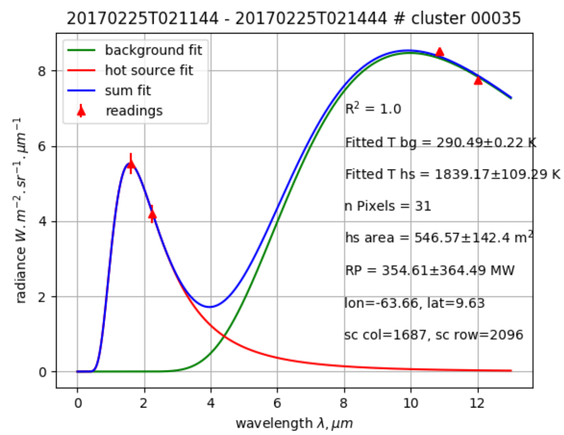
20170225T021144 - 20170225T021444 # cluster 00035
background fit
hot source fit
sum fit
readings
R^2 = 1.0
Fitted T bg = 290.49±0.22 K
Fitted T hs = 1839.17±109.29 K
n Pixels = 31
hs area = 546.57±142.4 m^2
RP = 354.61±364.49 MW
lon=-63.66, lat=9.63
sc col=1687, sc row=2096
radiance $W.m^{-2}.sr^{-1}.\mu m^{-1}$
wavelength $\lambda, \mu m$

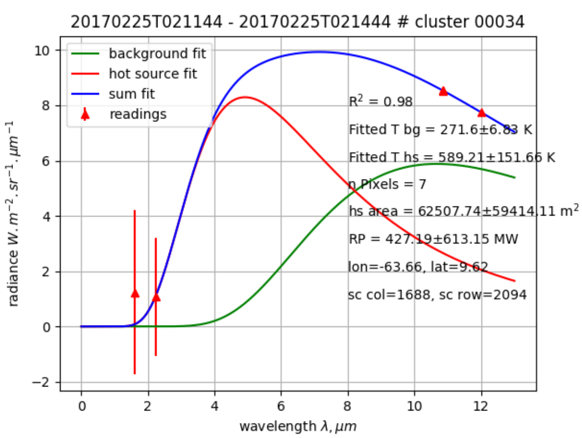
20170225T021144 - 20170225T021444 # cluster 00034
background fit
hot source fit
sum fit
readings
R^2 = 0.98
Fitted T bg = 271.6±6.83 K
Fitted T hs = 589.21±151.66 K
n Pixels = 7
hs area = 62507.74±59414.11 m^2
RP = 427.19±613.15 MW
lon=-63.66, lat=9.62
sc col=1688, sc row=2094
radiance $W.m^{-2}.sr^{-1}.\mu m^{-1}$
wavelength $\lambda, \mu m$

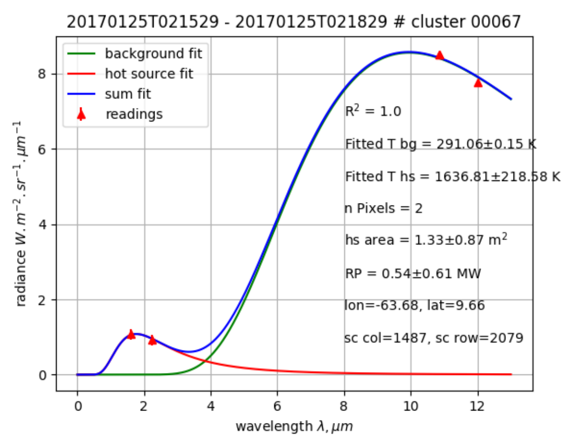
20170125T021529 - 20170125T021829 # cluster 00067
background fit
hot source fit
sum fit
readings
R^2 = 1.0
Fitted T bg = 291.06±0.15 K
Fitted T hs = 1636.81±218.58 K
n Pixels = 2
hs area = 1.33±0.87 m^2
RP = 0.54±0.61 MW
lon=-63.68, lat=9.66
sc col=1487, sc row=2079
radiance $W.m^{-2}.sr^{-1}.\mu m^{-1}$
wavelength $\lambda, \mu m$